ARCHIVES OF MECHANICS
Arch. Mech. **72** (4), 283–306, 2020, DOI: 10.24423/aom.3433

Analysis of multiple bifurcation behaviour for periodic structures

I. ARIO[1)], M. NAKAZAWA[2)]

[1)] *Department of Civil & Environmental Engineering, Hiroshima University, 1-4-1 Kagamiyama Higashi-hiroshima, Japan, e-mail: mario@hiroshima-u.ac.jp*

[2)] *Department of Civil and Environmental Engineering, Tohoku Gakuin University, Japan*

The classification of simple singularities in the post-buckling analysis of truss structures is well-known for elastic stability. To focus on multiple singularities including *a hilltop bifurcation point* (h-BP) and its bifurcation paths, we reviewed the multiple bifurcation analysis of *multi-folding microstructure* (MFM) models with periodic symmetry. Because the *Jacobian* at the h-BP of the MFM involves multiple 0-eigenvalues, it is challenging to analyse the bifurcation paths from the h-BP accurately. In this study, we investigated the multiple folding mechanism by analysing the neighbourhood of the h-BP and the *symmetric subgroups* of the geometric system in the two-dimensional plane and three-dimensional core of the MFM. We demonstrated that through the classification of multiple h-BP and bifurcation paths, it is possible to determine the unknown bifurcation equilibrium paths following h-BP, based on the *Jacobian stability* and the mechanism of *symmetric subgroups* in group theory containing the relationships between the primary path and the known bifurcation path(s) in the MFM system with periodic symmetry.

Key words: periodic symmetry, post-buckling analysis, multiple bifurcation, hill-top bifurcation, multi-folding microstructure.

1. Introduction

Fundamental mechanisms for the global and local (un-)stabilities based on geometrically periodic micro-macro structures and materials such as porous bodies, honeycomb [1–7], or a new resolving method of finite element method for the periodic scissors structure [8], between the scales of atomic lattice structure and periodic deformation pattern of geological folding under compression loading were reviewed from a post-buckling perspective. This folding phenomenon, in nonlinear mechanics, appears beyond the physics of scales problem as multi-body dynamics [9, 11]. From the viewpoint of multi-body physics issues, the structure is assumed to be the mechanical model of *the multi-folding microstructure* (MFM) [10, 11, 12], in a closed boundary condition.

The main purpose of this study is to clarify the structure of multiple bifurcation points, as well as that of bifurcation paths. This was achieved by tracking

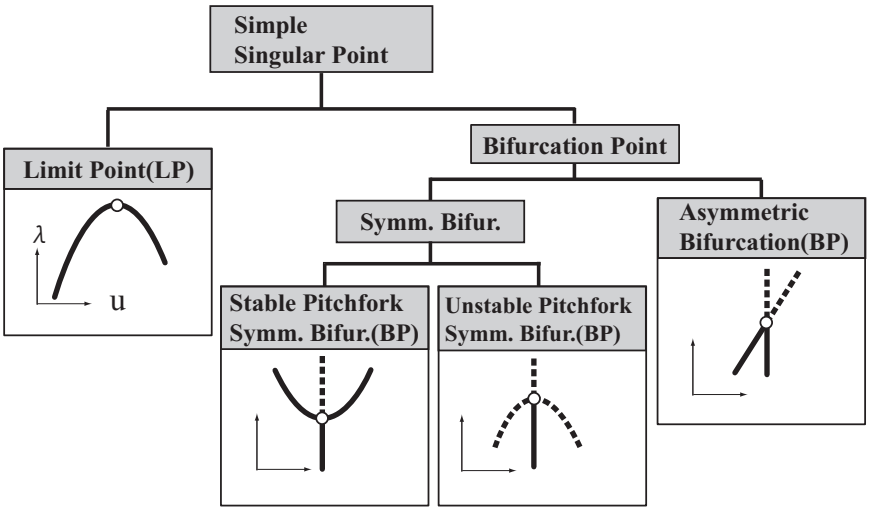

Fig. 1. Classification of simple singular point.

the nonlinear bifurcation behaviour of the folding phenomenon in the direction of the main axis of the applied load. The analysed structure was a multi-layer truss with pin-supported joints, without horizontal displacements. Additionally, the structure was allowed to fold to a stable state through sequential unstable states, such as snap-through or snap-back phenomena. Deflections were considered to be in range of large-deformation. The classification of a single singular point as a limit point, symmetry/asymmetry or stable/unstable bifurcation is well-known, as shown in Fig. 1. A hilltop branching point occurs as a result of collinearity of a limit point and many arbitrary bifurcation points of finite-dimensional, elastic, conservative, and equivariant systems, to its symmetry. Mathematical approaches have been presented by many scientists for these multiple h-BP problems, such as the group theory, stochastic approach, asymptotic method for bifurcation equations, perturbation method, and imperfection sensitivity, in static singular analysis [13–20]. The mechanical and elastic models of *the multi-folding microstructure* (MFM) were derived for finite dimensional elastic conservative systems, exhibiting hilltop branching at which many arbitrary bifurcation points coincided with a limit point. We investigated the classification and/or homoclinic bifurcation and chaos attractor in elastic two-bar truss with a symmetric structure [21]. The imperfection sensitivity with the h-BP point displayed complex phenomena of the geometrical nonlinearlity of the multi-folding elastic model. We also investigated the structural instability of the multiple symmetry bifurcation paths from the hilltop limit point in the MFM model with periodic symmetry and/or loss-symmetry [22, 23].

To discover the multiple bifurcation points as the critical load in theoretical folding mechanics, a method for obtaining the bifurcation paths of a discrete structural system with nonlinear equilibrium equations was studied by [24, 25]. In these papers, they referred to *the hilltop-bifurcation behaviour* of a three-layer plane truss subjected to a vertical loading at the top node. A comment was also given, without any proof, for the existence of an infinite number of multiple snap-through behaviours for a multiple-layered pantograph truss system. Additionally, the h-BP and bifurcation paths for the system were also studied. We are more interested in a system which is made of three-dimensional space, even though it is a simple model, because there may be more complex and strange phenomena in nonlinear mechanics. Thus, higher geometric symmetry tends to yield a greater number of bifurcation paths.

This paper presents our investigation for the bifurcation behaviour of the periodic symmetric truss, as shown in Fig. 2. Our prime concern is to know why there were more interesting bifurcation paths for this folding truss. The bifurcation behaviour of a diamond space truss was studied as a simplified folding model. Because the main objective of our study was the bifurcation behaviour of a symmetric truss with the axis line, the Euler buckling of each member was disregarded, i.e. it was assumed not to occur.

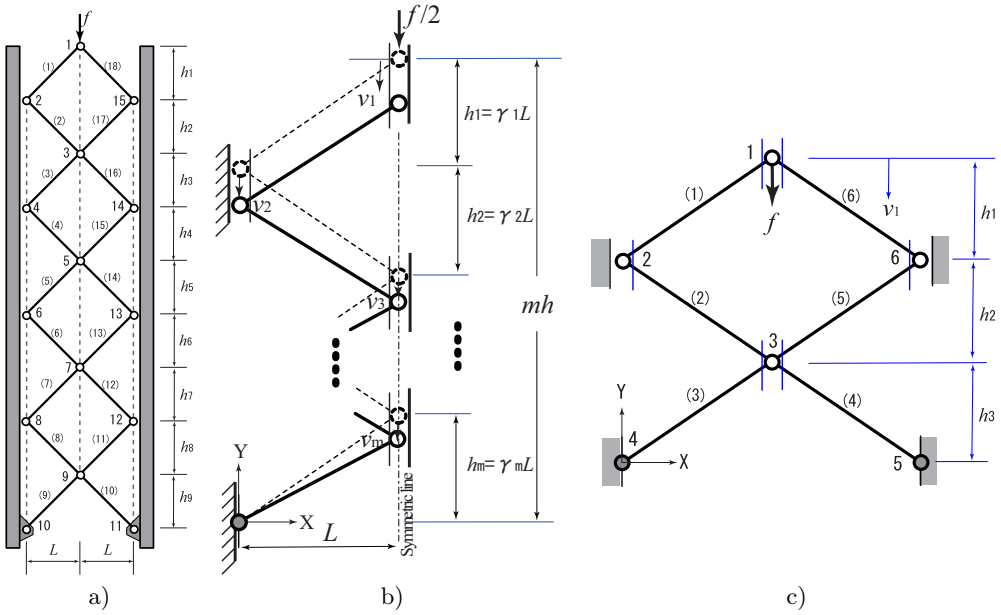

FIG. 2. Multi-folding pantographic systems; a) multi-layer model, b) one half of multi-layer model, c) basic 3-layer model.

2. Theory of elastic folding

In this section, we consider the folding mechanisms for the periodic linked truss structure, subjected to a vertical load at the top node, as shown in Fig. 2. The system is a pin-jointed elastic truss, and all nodes of the system displace vertically only. No allowance is made for friction or gravity for this geometrically nonlinear problem.

2.1. Theoretical approach for multi-folding truss on 2D

We assume a periodic height for each layer of $h_i = \gamma_i L$, where the width L of the truss is fixed. Therefore, an initial length for each bar in the geometry of the figure is expressed as

$$\ell_i = \sqrt{L^2 + h_i^2} = L\sqrt{1+\gamma_i^2} \quad \text{for } i = 1, \ldots, m. \tag{2.1}$$

The deformed length of each bar denoted as $\hat{\ell}_i$, is a function of the height and the nodal displacement variables

$$\hat{\ell}_1 = L\sqrt{1+(\gamma_1 - \bar{v}_1 + \bar{v}_2)^2}, \tag{2.2}$$

$$\vdots$$

$$\hat{\ell}_i = L\sqrt{1+(\gamma_i - \bar{v}_i + \bar{v}_{i+1})^2}, \tag{2.3}$$

$$\vdots$$

$$\hat{\ell}_m = L\sqrt{1+(\gamma_m - \bar{v}_m)^2} \tag{2.4}$$

where $\gamma_i = h_i/L > 0$, $\bar{v}_i = v_i/L$, $(i = 1, \cdots, m)$ and $\bar{v}_{m+1} = 0$ because the bottom node is translationally fixed.

Using Green's expression for strain, it is shown in each bar as

$$\varepsilon_i \equiv \frac{1}{2}\left\{\left(\frac{\hat{\ell}_i}{\ell_i}\right)^2 - 1\right\} \quad \text{for } i = 1, \ldots, m. \tag{2.5}$$

Substituting Eq. (2.1) to Eq. (2.4) into Eq. (2.5) we obtain

$$\varepsilon_i = \frac{1}{2}\left\{\frac{1+(\gamma_i - \bar{v}_i + \bar{v}_{i+1})^2}{1+\gamma_i^2} - 1\right\} \quad \text{for } i = 1, \ldots, m. \tag{2.6}$$

The total potential energy, $\mathcal{V}$, of the half model, subject to loading $f/2$ is then

given by

$$\mathcal{V} = \sum_{i=1}^{m} \frac{EA_i\ell_i}{2}(\varepsilon_i)^2 - \frac{f}{2}\bar{v}_1 L \tag{2.7}$$
$$= \sum_{i=1}^{m} \frac{EA_i L\sqrt{1+\gamma_i^2}}{2}\frac{1}{4}\left\{\frac{1+(\gamma_i-\bar{v}_i+\bar{v}_{i+1})^2}{1+\gamma_i^2}-1\right\}^2 - \frac{f}{2}\bar{v}_1 L.$$

For the case when $\gamma_i = \gamma$ $(i = 1,\ldots,m)$ and $EA_i = EA$ $(i = 1,\ldots,m)$ the total potential energy can be written as

$$\mathcal{V} = \frac{\kappa L}{8}\sum_{i=1}^{m}(\bar{v}_i-\bar{v}_{i+1})^2\left((\bar{v}_i-\bar{v}_{i+1})-2\gamma\right)^2 - \frac{f}{2}\bar{v}_1 L \tag{2.8}$$

where the stiffness parameter $\kappa = EA/(1+\gamma^2)^{3/2}$ (i.e. κ is a function of γ). From Eq. (2.8), we can obtain the equilibrium equations based on the principle of minimum energy [24] in the following way:

$$F_i(\ldots,v_i,\ldots) \equiv \frac{\partial\mathcal{V}}{\partial v_i} = \frac{\partial\mathcal{V}}{\partial\bar{v}_i}\frac{\partial\bar{v}_i}{\partial v_i} = 0, \quad \text{for } i = 1,\ldots,m. \tag{2.9}$$

Hence, for the 1st, $i-$th and $m-$th equilibrium equations are

$$F_1(\bar{v}_1,\bar{v}_2) = \frac{\kappa}{2}(\bar{v}_1-\bar{v}_2)((\bar{v}_1-\bar{v}_2)-\gamma)((\bar{v}_1-\bar{v}_2)-2\gamma)-\frac{f}{2} = 0, \tag{2.10}$$
$$F_i(\bar{v}_{i-1},\bar{v}_i,\bar{v}_{i+1}) = -\frac{\kappa}{2}(\bar{v}_{i-1}-\bar{v}_i)((\bar{v}_{i-1}-\bar{v}_i)-\gamma)((\bar{v}_{i-1}-\bar{v}_i)-2\gamma) \tag{2.11}$$
$$+\frac{\kappa}{2}(\bar{v}_i-\bar{v}_{i+1})((\bar{v}_i-\bar{v}_{i+1})-\gamma)((\bar{v}_i-\bar{v}_{i+1})-2\gamma) = 0,$$
$$F_m(\bar{v}_{m-1},\bar{v}_m) = -\frac{\kappa}{2}(\bar{v}_{m-1}-\bar{v}_m)((\bar{v}_{m-1}-\bar{v}_m)-\gamma)((\bar{v}_{m-1}-\bar{v}_m)-2\gamma) \tag{2.12}$$
$$+\frac{\kappa}{2}\bar{v}_m(\bar{v}_m-\gamma)(\bar{v}_m-2\gamma) = 0.$$

By using the implicit function theorem, it is then possible to solve for all variables $\bar{v}_i$, $(i = m,\ldots,1)$ as follows:

$$F_m(\bar{v}_{m-1},\bar{v}_m) = 0 \rightarrow \bar{v}_m = \mathcal{F}_m(\bar{v}_{m-1}), \tag{2.13}$$
$$F_i(\bar{v}_{i-1},\bar{v}_i,\bar{v}_{i+1}) = F_i(\bar{v}_{i-1},\bar{v}_i,\mathcal{F}_{i+1}(\bar{v}_i)) = 0 \rightarrow \bar{v}_i = \mathcal{F}_i(\bar{v}_{i-1}), \tag{2.14}$$
$$F_1(\bar{v}_1,\bar{v}_2) = F_1(\bar{v}_1,\mathcal{F}_2(\bar{v}_1)) = 0 \tag{2.15}$$

where $\mathcal{F}(\cdot)$ denotes a nonlinear function. Thus, we obtain all the solutions for each nonlinear equilibrium path by finding the normalised nodal displacements in turn.

Here, we consider the deformation relationship between the nodal displacement differences in the m-layer truss model. Up to the critical point, this overall deformation behaviour is assumed to be on the primary path. It is assumed that the deformation at the lowermost boundary condition in Fig. 2b) is 0, and that the arbitrary nodal displacements $\bar{v}_i$ and $\bar{v}_{i+1}$ are directly proportional to the displacement $\bar{v}_1$ at the top point. Based on the relationship between Eq. (2.13) and Eq. (2.15), the layers of the truss model are assumed to be homogeneous and of the same height:

$$(\bar{v}_i - \bar{v}_{i+1}) = \frac{m-i+1}{m}\bar{v}_1 - \frac{m-i}{m}\bar{v}_1 = \frac{1}{m}\bar{v}_1, \tag{2.16}$$

where

$$\begin{aligned} \bar{v}_i &= \frac{m-i+1}{m}\bar{v}_1, \quad i = 2, \ldots, m, \\ \bar{v}_{i+1} &= \frac{m-i}{m}\bar{v}_1, \quad i = 1, \ldots, m-1. \end{aligned}$$

An engineering problem arises when the proportional relation of Eq. (2.16) is satisfied until the singular point at which the structure is destabilized is reached.

2.2. Stability by Jacobian

The structural stability of the system can be determined from the eigenvalue of the tangent stiffness matrix, the *Jacobian* $J \in \mathbf{R}^{m\times m}$. If all the eigenvalues are positive, then the structure is considered to be stable, and if any eigenvalue has a negative value, then the structure is considered to be unstable. The stability of the structural system is determined from the singularity condition of the equilibrium equation having a singular point of displacements under the load parameter f. The stability of the system state is defined by the value of the determinant of the *Jacobian* J;

$$\det J(\bar{v}_i) \begin{cases} > 0: & \text{stable}, \\ = 0: & \text{critical}, \\ < 0: & \text{unstable}. \end{cases} \tag{2.17}$$

When the determinant at the critical point becomes zero, the number of null eigenvalues for the *Jacobian* is related to the number of singularities related to the structural instability. If, at the critical state, the number of null eigenvalues is one, the phenomenon is called a *simple singularity*. If there are two or more null eigenvalues, then the phenomenon is called *singularity multiplicity*, owing to the presence of *multi-singularity*. When the load has a point of maximum

intensity and multiple bifurcation points, this situation is called *hilltop type multiple bifurcation point*, and is commonly referred to as 'h-BP'.

The tangent stiffness matrix of this system J is defined as follows:

$$J = \left(\frac{\partial^2 \mathcal{V}}{\partial v_i \partial v_j}\right) = \left(\frac{\partial^2 \mathcal{V}}{\partial \bar{v}_i \partial \bar{v}_j}\frac{\partial \bar{v}_i}{\partial v_i}\frac{\partial \bar{v}_j}{\partial v_j}\right) = \left(\frac{\partial F_i}{\partial \bar{v}_j}\frac{\partial \bar{v}_j}{\partial v_j}\right) \quad \text{for } i,j = 1,\dots,m, \tag{2.18}$$

$$= \frac{\kappa}{2L}\begin{pmatrix} J_{1,2} & -J_{1,2} & & & \mathrm{O} \\ -J_{1,2} & J_{1,2}+J_{2,3} & -J_{2,3} & & \\ & -J_{2,3} & J_{2,3}+J_{3,4} & \ddots & \\ & & \ddots & \ddots & -J_{m-1,m} \\ \mathrm{O} & & & -J_{m-1,m} & J_{m-1,m}+J_{m,m} \end{pmatrix}$$

where $J_{i,j}$ is defined by the following;

$$J_{i,i+1} = 3(\bar{v}_i - \bar{v}_{i+1})^2 - 6(\bar{v}_i - \bar{v}_{i+1})\gamma + 2\gamma^2, \quad i = 1,\dots,m-1, \tag{2.19}$$

$$J_{m,m} = 3\bar{v}_m^2 - 6\bar{v}_m\gamma + 2\gamma^2. \tag{2.20}$$

Jacobian on the primary path. The Jacobian on the primary path, expressed by $\bar{v}_i$, can be derived from the sequential equations. The sequential equations are based on the proportional relationship between the nodal displacement differences. These sequential equations can be represented in each layer of the model as follows. Using Eq. (2.16) and Eq. (2.20), $J_{i,j}$ is defined as follows:

$$J_{i,i+1} = 3\left(\frac{\bar{v}_1}{m}\right)^2 - 6\left(\frac{\bar{v}_1}{m}\right)\gamma + 2\gamma^2, \quad i = 1,\dots,m-1 \tag{2.21}$$

$$J_{m,m} = 3\left(\frac{\bar{v}_1}{m}\right)^2 - 6\left(\frac{\bar{v}_1}{m}\right)\gamma + 2\gamma^2. \tag{2.22}$$

By substituting these components into the Jacobian (2.18), we obtain the following equation,

$$J(\bar{v}_1)|_{\mathrm{pr}} = \frac{\kappa}{2L}\left\{3\left(\frac{\bar{v}_1}{m}\right)^2 - 6\left(\frac{\bar{v}_1}{m}\right)\gamma + 2\gamma^2\right\}\begin{pmatrix} 1 & -1 & & & \mathrm{O} \\ -1 & 2 & -1 & & \\ & -1 & 2 & \ddots & \\ & & \ddots & \ddots & -1 \\ \mathrm{O} & & & -1 & 2 \end{pmatrix}. \tag{2.23}$$

The critical state of stability based on Eq. (2.17) is defined as

$$\det J(\bar{v}_1)|_{\mathrm{pr}} = \frac{\kappa}{2L}\left\{3\left(\frac{\bar{v}_1}{m}\right)^2 - 6\left(\frac{\bar{v}_1}{m}\right)\gamma + 2\gamma^2\right\} \times \det \begin{pmatrix} 1 & -1 & & & \mathrm{O} \\ -1 & 2 & -1 & & \\ & -1 & 2 & \ddots & \\ & & \ddots & \ddots & -1 \\ \mathrm{O} & & & -1 & 2 \end{pmatrix} = 0. \tag{2.24}$$

Then, the following condition is obtained:

$$3\left(\frac{\bar{v}_1}{m}\right)^2 - 6\left(\frac{\bar{v}_1}{m}\right)\gamma + 2\gamma^2 = 0. \tag{2.25}$$

From the condition of Eq. (2.25), a solution for the critical displacement $\bar{v}_1^{\mathrm{BP}}$ can be obtained by the following equation:

$$\bar{v}_1^{\mathrm{BP}} = \left\{\left(1 - \frac{1}{\sqrt{3}}\right)m\gamma, \left(1 + \frac{1}{\sqrt{3}}\right)m\gamma\right\}. \tag{2.26}$$

The state of this system is classified as

$$\begin{cases} \bar{v}_1 < \left(1 - \frac{1}{\sqrt{3}}\right)m\gamma\text{:} & \text{stable,} \\ \bar{v}_1 = \left(1 - \frac{1}{\sqrt{3}}\right)m\gamma\text{:} & \text{critical,} \\ \left(1 - \frac{1}{\sqrt{3}}\right)m\gamma < \bar{v}_1 < \left(1 + \frac{1}{\sqrt{3}}\right)m\gamma\text{:} & \text{unstable,} \\ \bar{v}_1 = \left(1 + \frac{1}{\sqrt{3}}\right)m\gamma\text{:} & \text{critical,} \\ \left(1 + \frac{1}{\sqrt{3}}\right)m\gamma < \bar{v}_1\text{:} & \text{stable.} \end{cases} \tag{2.27}$$

In Eq. (2.27), there is an unstable state on the primary path, between two critical displacements $\bar{v}_1^{\mathrm{BP}}$.

When the vertical displacement $\bar{v}_1$ at the top node reaches the critical value $\bar{v}_1^{\mathrm{BP}}$ on the primary path, the Jacobian of Eq. (2.23) becomes

$$J(\bar{v}_1^{\mathrm{BP}}) = \frac{\kappa}{2L}0\begin{pmatrix} 1 & -1 & & & \mathrm{O} \\ -1 & 2 & -1 & & \\ & -1 & 2 & \ddots & \\ & & \ddots & \ddots & -1 \\ \mathrm{O} & & & -1 & 2 \end{pmatrix} = \begin{pmatrix} 0 & 0 & & & \mathrm{O} \\ 0 & 0 & 0 & & \\ & 0 & 0 & \ddots & \\ & & \ddots & \ddots & 0 \\ \mathrm{O} & & & 0 & 0 \end{pmatrix}, \tag{2.28}$$

$$\lambda_i = 0,\ i = 1, \ldots m.$$

When the critical state is reached, all eigenvalues $\lambda_i, (i = 1, \ldots, m)$ are zero. In the critical state, eigenvalues correspond to an unstable state, where there are multiple bifurcations in the system.

In the general case, if the ideal folding truss had a multiple layer m, it would be possible to obtain the primary equilibrium equations. Let us consider the proportional relationship between the nodal displacements at the neighbourhood of Eqs.(2.10) or (2.15). If the nodal displacements of Eqs.(2.10) or (2.15) are used in Eq. (2.16), the load parameter $f(\bar{v}_1)$, including the maximum $f_{\max}$ at the top, equals the primary equilibrium path in the following:

$$
\begin{aligned}
f &= \kappa(\bar{v}_1 - \bar{v}_2)((\bar{v}_1 - \bar{v}_2) - \gamma)((\bar{v}_1 - \bar{v}_2) - 2\gamma) \\
&= \kappa \frac{\bar{v}_1}{m}\left(\frac{\bar{v}_1}{m} - \gamma\right)\left(\frac{\bar{v}_1}{m} - 2\gamma\right) \\
&= \frac{\kappa}{m^3}\bar{v}_1\left(\bar{v}_1 - m\gamma\right)\left(\bar{v}_1 - 2m\gamma\right),
\end{aligned} \tag{2.29}
$$

$$
f_{\max} = \frac{\kappa}{m^3}\bar{v}_1^{\mathrm{BP}}(\bar{v}_1^{\mathrm{BP}} - m\gamma)(\bar{v}_1^{\mathrm{BP}} - 2m\gamma) \quad \text{at } \bar{v}_1^{\mathrm{BP}} = \left(1 - \frac{1}{\sqrt{3}}\right)m\gamma. \tag{2.30}
$$

In this way, it is possible to express and generalize the equilibrium equations of the main path in the truss model. The considered truss model comprises m layers with a periodic structure.

2.3. Bifurcation analysis for three layers model ($m = 3$)

It is determined the equilibrium paths for the basic model, shown in Fig. 2c). The height of each layer was identical, i.e. $h_i = h$, hence $\gamma_i = \gamma$. To solve the variable $\bar{v}_i$, we used the implicit function theorem and substituted $m = 3$ into Eqs.(2.12) and (2.13), which gave the solution as follows:

$$
\bar{v}_3 = \mathcal{F}_3(\bar{v}_2)\begin{cases} = \bar{v}_2/2 & \text{for primary path,} \\ = \frac{1}{2}\left(\bar{v}_2 \pm \sqrt{-3\bar{v}_2^2 + 12\gamma\bar{v}_2 - 8\gamma^2}\right) & \text{for bif. paths,} \end{cases} \tag{2.31}
$$

$$
\bar{v}_2 = \mathcal{F}_2(\bar{v}_1)\begin{cases} = 2\bar{v}_1/3 & \text{for primary path,} \\ = -\gamma + \bar{v}_1 \pm \frac{\sqrt{3}}{3}\sqrt{-(\bar{v}_1 - \gamma)(\bar{v}_1 - 5\gamma)} & \text{for bif. paths.} \end{cases} \tag{2.32}
$$

From the use of the implicit function theorem (2.15) and/or (2.10) for $\bar{v}_1$ hence it is seen that the relationship between the load parameter and the displacement $\bar{v}_1$ was nonlinear

$$
f = \kappa\, \mathcal{F}_1(\bar{v}_1). \tag{2.33}
$$

Using $\bar{v}_2 = \mathcal{F}_2(\bar{v}_1)$ and $\bar{v}_3 = \mathcal{F}_3(\bar{v}_2)$, we could then express the equilibrium equations for the primary and bifurcation paths in terms of variable $\bar{v}_1$, as follows:

$$f_{\mathrm{pr}} = \kappa \frac{\bar{v}_1}{3}\left(\frac{\bar{v}_1}{3} - \gamma\right)\left(\frac{\bar{v}_1}{3} - 2\gamma\right) \quad \text{for primary path,} \tag{2.34}$$

$$f_{\mathrm{bf1}} = \pm \frac{\kappa}{3\sqrt{3}} \sqrt{-(\bar{v}_1 - \gamma)(\bar{v}_1 - 5\gamma)} \cdot (\bar{v}_1 - 2\gamma)(\bar{v}_1 - 4\gamma) \quad \text{for bif. paths.} \tag{2.35}$$

The equilibrium solutions f_{pr} and f_{bf1} are solved for $\bar{v}_1$; f_{bf1} represents a symmetric bifurcation path. In this system, the other asymmetric bifurcation path f_{bf2} exhibits half of the whole stiffness after bifurcation has occurred. This is due to the asymmetric deformation mode, which breaks the left-right symmetry, leading to half the sum of Eq. (2.34) and Eq. (2.35), which is represented by the following equation:

$$f_{\mathrm{bf2}}(\bar{v}_1) = \frac{f_{\mathrm{pr}}(\bar{v}_1) + f_{\mathrm{bf1}}(\bar{v}_1)}{2} \quad \text{for asymmetric bif. path.} \tag{2.36}$$

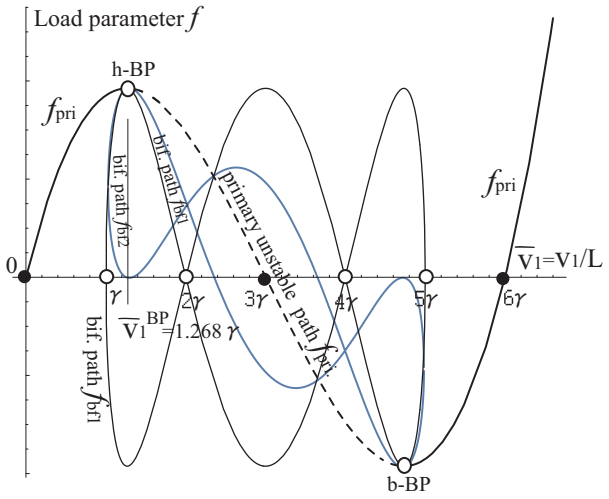

FIG. 3. Nonlinear equilibrium paths using Eqs. (2.34)–(2.36).

The different equilibrium paths, such as $f_{\mathrm{pr}}, f_{\mathrm{bf1}}$ and f_{bf2}, from Eq. (2.34) to Eq. (2.36), are depicted in Fig. 3. In Fig. 3, the dotted line on the primary path represents the unstable state. The unstable state is considered to occur from the minimum value, at the 'b-BP' of the bottom node, to the maximum load at the limit point (h-BP). The main path f_{pr} becomes zero at the centre of the instability, when $\bar{v}_1 = 3\gamma$ equals the height of the three-layer truss model.

When the vertical displacement $\bar{v}_1$ reaches the critical displacement $\bar{v}_1^{\mathrm{BP}}$ at the top node, the load parameter becomes $f_{\max}$ at the same h-BP. Moreover, the equilibrium path is changed from the main equilibrium path f_{pr} to one of the several bifurcation paths f_{bf} at the limit and a bifurcation point. This is called *the hilltop-bifurcation point*, and is defined as $f_{\max} = f_{\mathrm{pr}}(\bar{v}_1^{\mathrm{BP}}) = f_{\mathrm{bf}}(\bar{v}_1^{\mathrm{BP}})$. Therefore, at the critical displacement $\bar{v}_1^{\mathrm{BP}}$, the relationship between the primary path f_{pr}, including the load parameter, and the bifurcation path f_{bf} corresponds to multiple equilibrium states as $f_{\mathrm{pr}}(\bar{v}_1^{\mathrm{BP}}) = f_{\mathrm{bf1}}(\bar{v}_1^{\mathrm{BP}}) = f_{\mathrm{bf2}}(\bar{v}_1^{\mathrm{BP}})$.

The gradients at the top point (h-BP) for the all equilibrium paths are smooth and can be represented by $df/d\bar{v}_1 = 0$, as shown in Fig. 3. This relationship is valid to both before and after h-BP. In Fig. 3, it can be observed that two bifurcation paths f_{bf1} from h-BP pass through the marks of '$\circ$'. Also presenting asymmetric deformation, two bifurcation paths f_{bf2} from h-BP are indicated by the thin blue lines in Fig. 3. Using bifurcation analysis, and based on the structural stability of the post-buckling problem, it is realised that there are the multiple limit and bifurcation points. These points can be, for example, the h-BP, and may occur in many harmonic equilibrium paths in geometric nonlineariity. The limit and bifurcation points may occur in trusses with multiple microstructures, including periodically symmetric folding systems.

From the equation of the Jacobian (2.23), considering the generalized representation of the m layer, the tangential stiffness matrix of the three-layer truss J can be systematically obtained. The characteristic equation of expression (2.38) can be represented by the following:

$$J(v_i) = \frac{\kappa}{2L}\left\{3\left(\frac{\bar{v}_1}{3}\right)^2 - 6\left(\frac{\bar{v}_1}{3}\right)\gamma + 2\gamma^2\right\}\begin{pmatrix} 1 & -1 & 0 \\ -1 & 2 & -1 \\ 0 & -1 & 2 \end{pmatrix}, \tag{2.37}$$

$$\det|J-\lambda I| = \frac{\kappa}{2L}\left\{3\left(\frac{\bar{v}_1}{3}\right)^2 - 6\left(\frac{\bar{v}_1}{3}\right)\gamma + 2\gamma^2\right\}(-\lambda^3+5\lambda^2-6\lambda+1) = 0. \tag{2.38}$$

From the characteristic equation (2.38), three eigenvalues λ_i depend on $\bar{v}_1$ Fig. 4 depicts the result of the solution curve. In this figure, when the displacement $\bar{v}_1$ reaches its critical value, $\bar{v}_1^{\mathrm{BP}}$, all three eigenvalues are zero, indicating the existence of multiple solutions.

The critical displacement of the formula (2.26) can be obtained by the following equation, in the case of $m = 3$:

$$\bar{v}_1^{\mathrm{BP}} = \{1.268\gamma, 4.732\gamma\}. \tag{2.39}$$

Since the eigenvalues are all null at $\bar{v}_1^{\mathrm{BP}} = 1.268\gamma$, it is impossible to solve the eigenvectors as their bifurcation modes. Therefore, in this system, we focus on

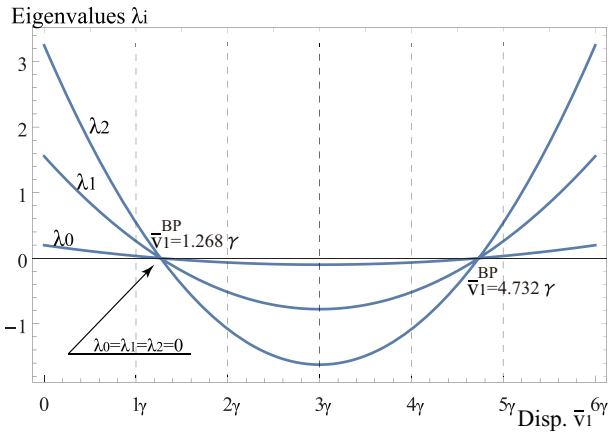

FIG. 4. Change of eigenvalues depends on $\bar{v}_1$ in $n = 3$ layers model.

the localization of the folding patterns of a truss with a multi-layer symmetric structure. Using the eigenvalue analysis near the critical displacement, just before destabilization, the normal eigenvectors for each eigenvalue are obtained Fig. 5a1), b1), c1). If the maximum value of the displacement changes locally in the vector, it can be understood that each folding pattern becomes different. Furthermore, the maximum nodal deformation after the bifurcation point is localized concentrically, as shown in Fig. 5a2), b2), c2a), c2b).

$$\begin{cases} \lambda_1, \lambda_2, \lambda_3 > 0, & \text{at } \bar{v}_1 < 1.268\gamma\text{: stable state,} \\ \lambda_1 = \lambda_2 = \lambda_3 = 0, & \text{at } \bar{v}_1 = 1.268\gamma\text{: multiple critical states.} \end{cases}$$

The maximum load at h-BP can be obtained as follows by applying $m = 3$ to the primary path of Eq. (2.30).

$$f_{\mathrm{pr}}^{\max} = f(\bar{v}_1^{\mathrm{BP}}) = +0.3849\kappa\gamma^3 \quad \text{at } \bar{v}_1^{\mathrm{BP}} = 1.268\gamma. \tag{2.40}$$

Alternatively, Eq. (2.34) can be used. The load parameter for the two bifurcation paths, f_{bf1} of Eq. (2.35) and f_{bf2} of Eq. (2.36), is traced at $\bar{v}_1^{\mathrm{BP}} = 1.268\gamma$;

$$\begin{aligned} f_{\mathrm{bf1}}(\bar{v}_1^{\mathrm{BP}}) &= \pm\frac{\kappa}{3\sqrt{3}}\sqrt{-(\bar{v}_1^{\mathrm{BP}} - \gamma)(\bar{v}_1^{\mathrm{BP}} - 5\gamma)} \cdot (\bar{v}_1^{\mathrm{BP}} - 2\gamma)(\bar{v}_1^{\mathrm{BP}} - 4\gamma) \\ &= \{+0.3849\kappa\gamma^3, -0.3849\kappa\gamma^3\}, \end{aligned} \tag{2.41}$$

$$\begin{aligned} f_{\mathrm{bf2}}(\bar{v}_1^{\mathrm{BP}}) &= \frac{f_{\mathrm{pr}}(\bar{v}_1^{\mathrm{BP}}) + f_{\mathrm{bf1}}(\bar{v}_1^{\mathrm{BP}})}{2} \\ &= \{+0.3849\kappa\gamma^3, 0\}. \end{aligned} \tag{2.42}$$

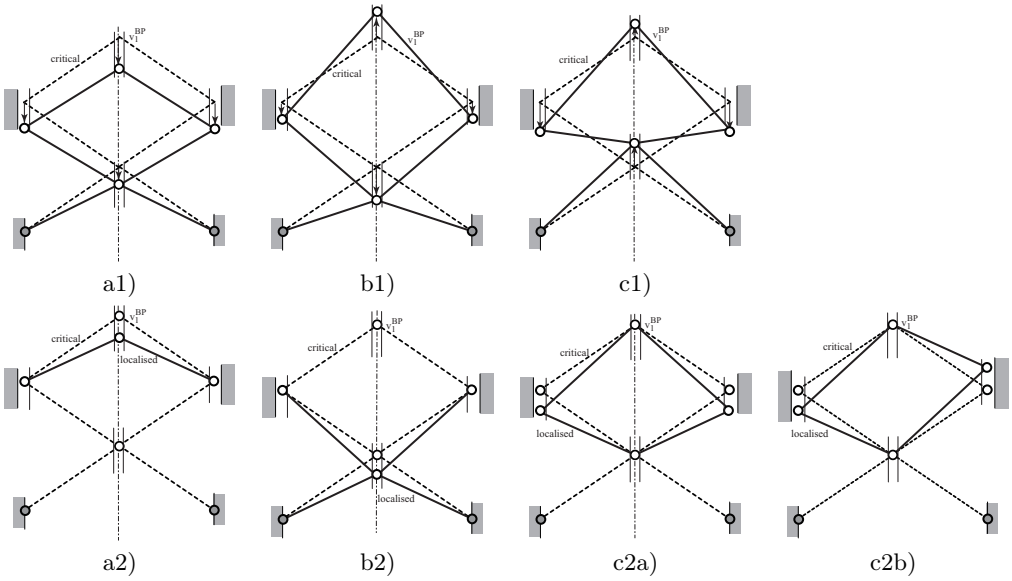

FIG. 5. Eigenvectors and the localised folding patterns: a1) eigenvector for λ_1, b1) eigenvector for λ_2, c1) eigenvector for λ_3, a2) local folding mode at the top node, b2) locally symmetric folding mode at the third node, c2a) locally symmetric folding mode at the second nodes, c2b) locally asymmetric folding mode at the second nodes.

In the different Eqs. (2.40)–(2.42), the load parameter in a three-layer model (2D), at $\bar{v}_1 = 1.268\gamma$, correspond to the same maximum value. In the calculations, the limit point and the bifurcation point, corresponding to the maximum load of the $f(\bar{v}_1^{\mathrm{BP}})$ curve, are consistent with each other. Therefore, $f_{\mathrm{pr}}(\bar{v}_1^{\mathrm{BP}}) = f_{\mathrm{bf}}(\bar{v}_1^{\mathrm{BP}})$ is also a critical point. As such, it was recognised as a bifurcation point.

From the stability analysis of the Jacobian, in a displacement-constrained 2D truss model of an m-layer pantograph with a periodic structure, there are multiple bifurcation points. In these bifurcation points, multiple null eigenvalues occur at a single critical displacement. All the singular points are coincident with the maximum and minimum points in the primary equilibrium path and bifurcation paths. Thus, it was found that, when the number of layers m is odd, the singular point is a hilltop multi-bifurcation point, with several symmetric patterns. In this paper, we calculated theoretically the proportional relationship of the main path equilibrium state and bifurcation paths from the Jacobian near the hilltop bifurcation point, however it is not available to obtain bifurcation hierarchy or more complex folding patterns of the MFM. Therefore, further analysis including the multi-degree of freedom of the periodic structure and/or the horizontal displacement behavior will be necessary. The multi-folding analysis of the three-dimensional core truss of the MFM is explained in next section.

3. Theoretical approach for multi-folding truss in 3D

We considered the folding mechanisms for a (pantographic) truss structure subject to a vertical load at the top node of the system, shown in Fig. 6. The system was a pin-jointed elastic truss and all nodes of the system displaced vertically only. No allowance was made for friction or gravity for this geometrically nonlinear problem. In addition, we believe that no Euler elastic buckling occurred for each bar by itself in this truss. We assumed a periodic height for each layer of $h_i = \gamma_i L$, where the width L of the truss was fixed. Therefore, the initial length of each bar in the geometry of the figure is expressed as

$$\ell_{(i),k} = \sqrt{L^2 + h_i^2} = L\sqrt{1+\gamma_i^2} \quad \text{for } k = 1, \ldots, n,\ i = 1, 2, \tag{3.1}$$

where n represents the number of polygonal model's members.

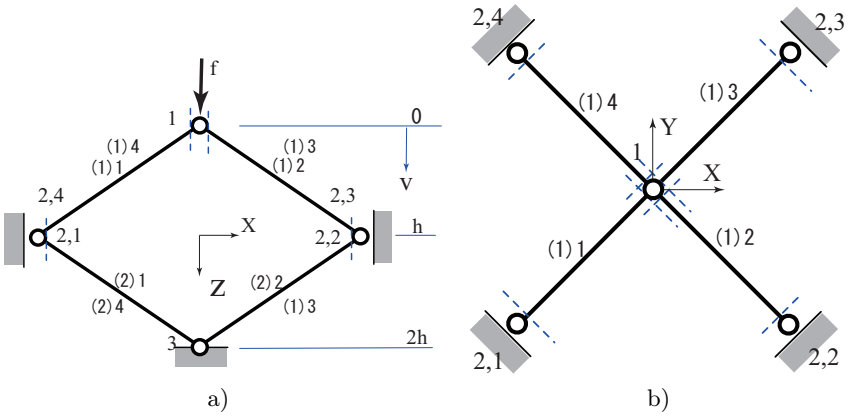

Fig. 6. Folding model in 3D; a) side view, b) plan view.

Using a definition of the Green strain, the potential strain energy for the up and down side of this model, $\mathcal{V}_i$, of the model shown in Fig. 6(a), subject to loading f^* is then given by

$$\mathcal{V}_1 = \frac{\kappa L}{8} \sum_{k=1}^{n} (\bar{v}_1 - \bar{v}_{2,k})^2 (\bar{v}_1 - \bar{v}_{2,k} - 2\gamma)^2, \tag{3.2}$$

$$\mathcal{V}_2 = \frac{\kappa L}{8} \sum_{k=1}^{n} (\bar{v}_{2,k})^2 (\bar{v}_{2,k} - 2\gamma)^2. \tag{3.3}$$

Here, it was assumed, as the condition for this model $\kappa = EA/(1+\gamma)^{3/2}$, $\gamma_i = \gamma$,

$\bar{v}_i = v_i/L$, $h_i = h$. The total potential energy is expressed as follows:

$$\begin{aligned}(3.4)\quad \mathcal{V} &= \mathcal{V}_1 + \mathcal{V}_2 - f\bar{v}_1 L \\ &= \frac{\kappa L}{8}\sum_{k=1}^{n}[(\bar{v}_1 - \bar{v}_{2,k})^2(\bar{v}_1 - \bar{v}_{2,k} - 2\gamma)^2 + (\bar{v}_{2,k})^2(\bar{v}_{2,k} - 2\gamma)^2] - f\bar{v}_1 L.\end{aligned}$$

We can obtain the equilibrium equations based on the principle of minimum energy in the following way:

$$(3.5)\qquad F_i(\ldots, v_i, \ldots) \equiv \frac{\partial \mathcal{V}}{\partial v_i} = \frac{\partial \mathcal{V}}{\partial \bar{v}_i}\frac{\partial \bar{v}_i}{\partial v_i} = 0 \quad \text{for } i = 1, \ldots, m.$$

For example for $\bar{v}_1$, it is shown as

$$\begin{aligned}(3.6)\quad F_1 &= \frac{\partial \mathcal{V}}{\partial \bar{v}_1}\frac{1}{L} = 0 \\ &= \frac{\kappa}{8}\sum_{k=1}^{n}\left\{\frac{\partial(\bar{v}_1-\bar{v}_{2,k})^2}{\partial \bar{v}_1}(\bar{v}_1-\bar{v}_{2,k}-2\gamma)^2+(\bar{v}_1-\bar{v}_{2,k})^2\frac{\partial(\bar{v}_1-\bar{v}_{2,k}-2\gamma)^2}{\partial \bar{v}_1}\right\}-f \\ &= \frac{\kappa}{4}\sum_{k=1}^{n}\left\{(\bar{v}_1-\bar{v}_{2,k})(\bar{v}_1-\bar{v}_{2,k}-2\gamma)^2+(\bar{v}_1-\bar{v}_{2,k})^2(\bar{v}_1-\bar{v}_{2,k}-2\gamma)\right\}-f \\ &= \frac{\kappa}{4}\sum_{k=1}^{n}(\bar{v}_1-\bar{v}_{2,k})(\bar{v}_1-\bar{v}_{2,k}-2\gamma)\left\{(\bar{v}_1-\bar{v}_{2,k})+(\bar{v}_1-\bar{v}_{2,k}-2\gamma)\right\}-f \\ &= \frac{\kappa}{2}\sum_{k=1}^{n}(\bar{v}_1-\bar{v}_{2,k})(\bar{v}_1-\bar{v}_{2,k}-\gamma)(\bar{v}_1-\bar{v}_{2,k}-2\gamma)-f = 0.\end{aligned}$$

The other shows

$$\begin{aligned}(3.7)\quad F_{2,k} &= \frac{\partial \mathcal{V}}{\partial \bar{v}_{2,k}}\frac{1}{L} = 0 \\ &= \frac{\kappa}{8}\left\{\frac{\partial(\bar{v}_1-\bar{v}_{2,k})^2(\bar{v}_1-\bar{v}_{2,k}-2\gamma)^2}{\partial v_{2,k}}+\frac{\partial(\bar{v}_{2,k})^2(\bar{v}_{2,k}-2\gamma)^2}{\partial v_{2,k}}\right\} \\ &= \frac{\kappa}{8}\{(-2)(\bar{v}_1-\bar{v}_{2,k})(\bar{v}_1-\bar{v}_{2,k}-2\gamma)^2+(\bar{v}_1-\bar{v}_{2,k})^2(-2)(\bar{v}_1-\bar{v}_{2,k}-2\gamma)^2 \\ &\quad +2\bar{v}_{2,k}(\bar{v}_{2,k}-2\gamma)^2+\bar{v}_{2,k}^2 2(\bar{v}_{2,k}-2\gamma)^2\} \\ &= \frac{\kappa}{4}\{-(\bar{v}_1-\bar{v}_{2,k})(\bar{v}_1-\bar{v}_{2,k}-2\gamma)2(\bar{v}_1-\bar{v}_{2,k}-\gamma)+\bar{v}_{2,k}(\bar{v}_{2,k}-2\gamma)2(\bar{v}_{2,k}-\gamma)\} \\ &= \frac{\kappa}{2}\{-(\bar{v}_1-\bar{v}_{2,k})(\bar{v}_1-\bar{v}_{2,k}-\gamma)(\bar{v}_1-\bar{v}_{2,k}-2\gamma)+\bar{v}_{2,k}(\bar{v}_{2,k}-\gamma)(\bar{v}_{2,k}-2\gamma)\} = 0, \\ &\qquad\qquad k = 1, \ldots, n.\end{aligned}$$

After this equation, let us consider the 3D model as $n = 4$.

The results obtained regarding the force versus displacement curves are depicted in Fig. 3 (or later Fig. 10). The force versus displacement curves were obtained considering that the system was subjected to a vertical load of increasing intensity, applied at the top point h-BP. This system consisted of multiple limit and bifurcation points, located in the elastic unstable state, outside the primary path. We can also refer to another relevant case, as shown in Ikeda *et al.* [18, Fig. 10, p. 762]. These results are similar to the force versus displacement curves of the two-bar truss model. The two-bar truss model presents bifurcations of the hilltop type, having several imperfection paths in their dimensional space. Thus, we may be able to foresee where there exist several folding and post-buckling patterns in this system. This can be performed based on symmetry-breaking laws, considering the subgroups of its symmetry. The degrees of freedom of this MFM system only allowed vertical displacements.

The loading displacement at the top node suddenly appeared large upon loading, and snap-through nonlinear behaviour was observed. At the critical displacement, there were four nodal points on the mid layer. There are typical deformation patterns in the dihedral group $\mathrm{D}_4 \in \mathrm{D}_\mathrm{n}$, in the vertical Z-direction. The dihedral group contains the subgroups of the initial regular n-gonal symmetry, $\mathrm{D}_4(=\mathrm{C}_{4\mathrm{v}})$ as shown in the following:

$$\text{subgroups: } \mathrm{D}_4, (\mathrm{C}_4,)\ \mathrm{D}_2^{\mathrm{k}},\ (\mathrm{C}_2,)\ \mathrm{D}_1^{\mathrm{j}}, \mathrm{C}_1 \quad \text{for } k = 1, 2,\ j = 1, \ldots, 4.$$

The relationship between several deformed patterns for each subgroup space of D_4 is shown in Fig. 7.

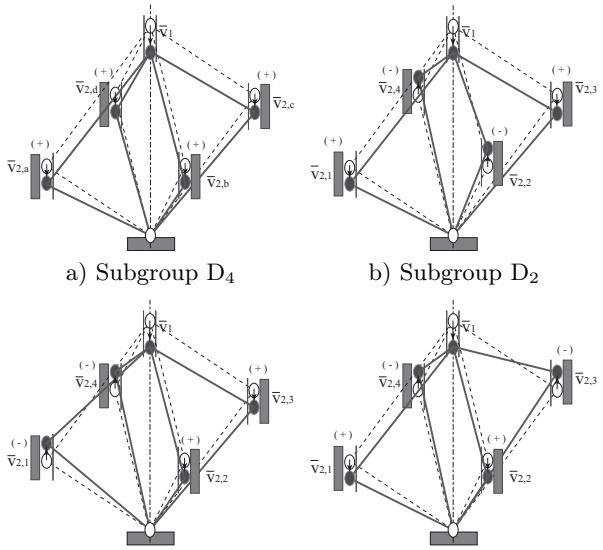

Fig. 7. Deformation patterns for 3D folding model.

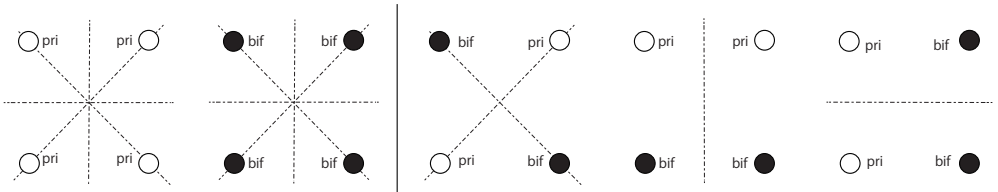

a) Subgroup D_4 b) Subgroup D_4 c) Subgroup D_2^2 d) Subgroup D_1 e) Subgroup D_1^3

FIG. 8. Corresponding to an order of solutions (○ and ● denote the linear and the nonlinear solutions, respectively, to be substituted).

The primary and bifurcation solutions are obtained by solving Eq. (3.7) as follows:

$$\bar{v}_{2,k} \begin{cases} = \bar{v}_1/2 & \text{for primary path,} \\ = \frac{1}{2}\big(\bar{v}_1 \pm \sqrt{-8\gamma^2 + 12\gamma\bar{v}_1 - 3\bar{v}_1^2}\,\big) & \text{for bifurcation path,} \end{cases} \quad \text{for } k = 1, \ldots, 4. \tag{3.8}$$

These solutions include the linear and nonlinear terms for each nodal displacement, $\bar{v}_{2,k}$. And, it was considered that several equilibrium paths were combined by these chosen solutions. Therefore, it was shown that there was a combination of linear and nonlinear solutions, such as ○ and ● as shown in Fig. 8. This figure represents a number of linear and nonlinear solutions for the nodal displacement, $\bar{v}_{2,k}$. For example, figure a) marked the layout for four nodal points, which correspond to the deformation pattern of the primary path, when the combination of all linear solutions is $\bar{v}_{2,k} = \bar{v}_1/2$. Figure b) marked the layout for four nodal points with nonlinear solutions after the h-BP. Figures c)–e) have two primary and nonlinear bifurcation solutions with symmetric subgroups, respectively.

3.1. Primary path and bifurcation paths

In the previous subsection, the three solutions for $\bar{v}_{2,k}$ were determined, and they were substituted into the equilibrium equations $\boldsymbol{F}_i$. There were several equilibrium paths to be satisfied for the combination of these solutions. Firstly, if all displacements equal the same linear relationship $\bar{v}_{2,k} = \bar{v}_1/2$ $(k = 1, \ldots, 4)$, as shown in Fig. 9a), Eq. (3.6) will be the fundamental equilibrium equation as the primary path in the following:

$$f_{\mathrm{pr}} = \frac{\kappa}{4}\bar{v}_1(\bar{v}_1 - 2\gamma)(\bar{v}_1 - 4\gamma). \tag{3.9}$$

This equation is the primary nonlinear path which has the D_4 symmetry of the same vertical displacements for $\bar{v}_{2,k}$. This deformation of the system is not symmetry-breaking of D_4, i.e. before D_4 symmetry-breaking.

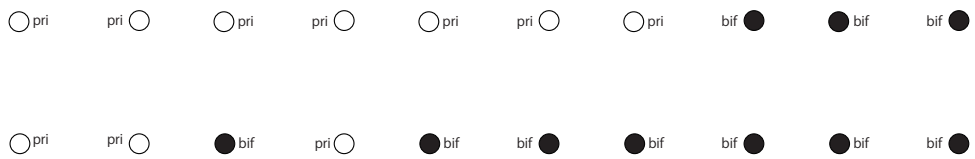

a) Primary path b) Bif. path 1 c) Bif. path 2 d) Bif. path 3 e) Bif. path 4

FIG. 9. Corresponding to an order of solutions ('○' and '●' denote the linear and nonlinear solutions, respectively, to be substituted).

Secondly, there were several bifurcation paths under the condition of solution's combination shown in Fig. 9b) in the following:

$$\bar{v}_{2,2} = \bar{v}_{2,3} = \bar{v}_{2,4} = \bar{v}_1/2,\ \bar{v}_{2,1} = \frac{1}{2}\Big(\bar{v}_1 - \sqrt{-8\gamma^2 + 12\bar{v}_1\gamma - 3\bar{v}_1^2}\Big),$$

$$f_{\mathrm{bf1}} = \frac{\kappa}{16}(48\gamma^3 - 64v_1\gamma^2 + 30v_1^2\gamma - 5v_1^3) \quad \text{for bif. path 1.} \tag{3.10}$$

Next, the condition of another combination of solutions, including two nonlinear solutions, shown in Fig. 9c) is given as follows:

$$\bar{v}_{2,3} = \bar{v}_{2,4} = \bar{v}_1/2,\ \bar{v}_{2,1} = \bar{v}_{2,2} = \frac{1}{2}\Big(\bar{v}_1 - \sqrt{-8\gamma^2 + 12\bar{v}_1\gamma - 3\bar{v}_1^2}\Big),$$

$$f_{\mathrm{bf2}} = \frac{\kappa}{8}(48\gamma^3 - 80v_1\gamma^2 + 42v_1^2\gamma - 7v_1^3) \quad \text{for bif. path 2.} \tag{3.11}$$

Two nonlinear solutions shown in Fig. 9c) are corresponding to the bifurcation equilibrium paths in Figs. 8c)–e).

With an increasing number of nonlinear solutions for substituting into Eq. (3.6), there is one remaining linear relationship for $\bar{v}_{2,k}$, shown in Fig. 9d);

$$\bar{v}_{2,4} = \bar{v}_1/2, \quad \bar{v}_{2,1} = \bar{v}_{2,2} = \bar{v}_{2,3} = \frac{1}{2}\Big(\bar{v}_1 - \sqrt{-8\gamma^2 + 12\bar{v}_1\gamma - 3\bar{v}_1^2}\Big),$$

$$f_{\mathrm{bf3}} = \kappa\left(9\gamma^3 - 16v_1\gamma^2 + \frac{69{v_1}^2\gamma}{8} - \frac{23{v_1}^3}{16}\right) \quad \text{for bif. path 3.} \tag{3.12}$$

Finally, substituting all the nonlinear solutions into Eq. (3.6), we obtained the following relationship, shown in Fig. 9e);

$$\bar{v}_{2,1} = \bar{v}_{2,2} = \bar{v}_{2,3} = \bar{v}_{2,4} = \frac{1}{2}\Big(\bar{v}_1 - \sqrt{-8\gamma^2 + 12\bar{v}_1\gamma - 3\bar{v}_1^2}\Big)$$

$$f_{\mathrm{bf4}} = 2\kappa(6\gamma^3 - 11v_1\gamma^2 + 6v_1^2\gamma - v_1^3) \quad \text{for bif. path 4.} \tag{3.13}$$

It corresponds to the deformation pattern of the 4th bifurcation path. This equilibrium path is the most unstable state from h-BP.

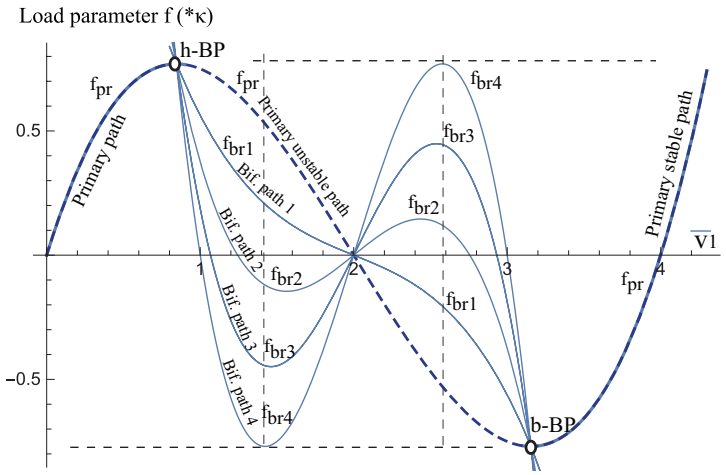

FIG. 10. Primary path and bifurcation paths ($m = 2$, $n = 4$, $\gamma = 1$).

These relationships are plotted in Fig. 10 as bifurcation paths from the first h-BP. It is known that there are several different unstable paths between h-BP and b-BP. The loss of the load parameter from h-BP depends on the number of nonlinear solutions as '•', i.e. when all solutions are linear, it corresponds to the primary unstable path. However, when all solutions are nonlinear, it corresponds to the most decreasing unstable bifurcation path (bif. path 4 in Fig. 10). for this simple model in three dimensions. All paths go through the center position $\bar{v}_1 = 2$.

In general, the number of all bifurcation paths is n and then the equation is defined $f_{\mathrm{bf}n}$ from f_{bf4} in case of $n = 4$. We obtained the following law from the relationship between the primary path f_{pr} and bifurcation paths $f_{\mathrm{bf}i}$.

$$f_{\mathrm{bf}i} = \frac{(n-i)f_{\mathrm{pr}} + i f_{\mathrm{bf}n}}{n}, \qquad i = 1, \ldots, n. \tag{3.14}$$

In case of $n = 4$, any bifurcation path $f_{\mathrm{bf}i}$ shows from f_{pr} and f_{bf4} of Eq. (3.14) in the following;

$$f_{\mathrm{bf1}} = \frac{3f_{\mathrm{pr}} + f_{\mathrm{bf4}}}{4}, \tag{3.15}$$

$$f_{\mathrm{bf2}} = \frac{f_{\mathrm{pr}} + f_{\mathrm{bf4}}}{2}, \tag{3.16}$$

$$f_{\mathrm{bf3}} = \frac{f_{\mathrm{pr}} + 3f_{\mathrm{bf4}}}{4}. \tag{3.17}$$

These bifurcation paths correspond to the analytical results in Fig. 10 (Refer Fig. 11a)). We realised that if one of these relationships was obtained from

experimental data, consequently, there would be a bifurcation path and a number of bifurcation solutions which depend on the influence of the lost load resistance.

3.2. Classification of hilltop type multiple bifurcation points

As a result of the nonlinear equilibrium path of the three-layer periodic MFM truss Fig. 3, it was confirmed that there were a h-BP point and bifurcation paths from h-BP. It is predicted that more unstable bifurcation paths are derived in periodic structures with three or more layers. This suggests the existence of multiple singularities and multiple different symmetric and unstable branch paths in the periodic structure system. If the bifurcation path is stable, it becomes a symmetric and stable type of h-BP. In the results of the nonlinear equilibrium path of the two-layer core truss shown in Fig. 10, consisting of 4-bars in the 3D space, we focused on the bifurcation path in the hierarchical subgroup with D_4-symmetry. By substituting the solution '$\circ$' and the bifurcated solution '$\bullet$' into the bifurcation equation, unstable bifurcation paths arose from several different h-BP. As a result of determining bifurcation paths of interesting behaviour, those of the three-layer MFM truss with symmetric group D_2 were found to be unstable. Moreover, the foldings present bifurcation patterns with symmetric subgroup D_1 and asymmetric subgroup C_2. If the number of layers in the MFM system is odd, the bifurcation paths at the h-BP exhibit the smoothness limit point similar to that of the shape of the primary path. In contrast, if the number of layers is even, the bifurcation paths cross each other at the h-BP. From the analysis and results regarding bifurcation, it is realised that the number of layers is different, depending on the branch type of the bifurcation paths. However, we realised that the number and position of the bifurcation solutions associated to those bifurcation paths, corresponded to part of the D_4- subgroup. Thus, the system was not completely asymmetric. In fact, the system had an unstable path, presenting a D_4 symmetric subgroup.

In summary, the classification and characteristics of multiple hilltop bifurcation points in a periodic structure system can be drawn as shown in the bifurcation diagram Fig. 11. This can be done similarly to the results for the 3D diamond truss, in the case of an even number of layers. Fig. 11a) shows a type of bifurcation, in which a plurality of unstable asymmetric bifurcation paths arose the loss of the number of the stiffness from h-BP. Fig. 11b) shows unstable symmetric multiple bifurcation paths from h-BP in odd number m layers. Fig. 11c), shows an even number of layer truss, where it is possible to see multiple symmetrically unstable parabola and asymmetric bifurcation paths from h-BP in the MFM system of 3D. It is shown in the results regarding the bifurcation of the MFM truss, with the multiple number layers, that the existence of bifurcation can be systematically inferred. If we considered the 3D case with imperfections,

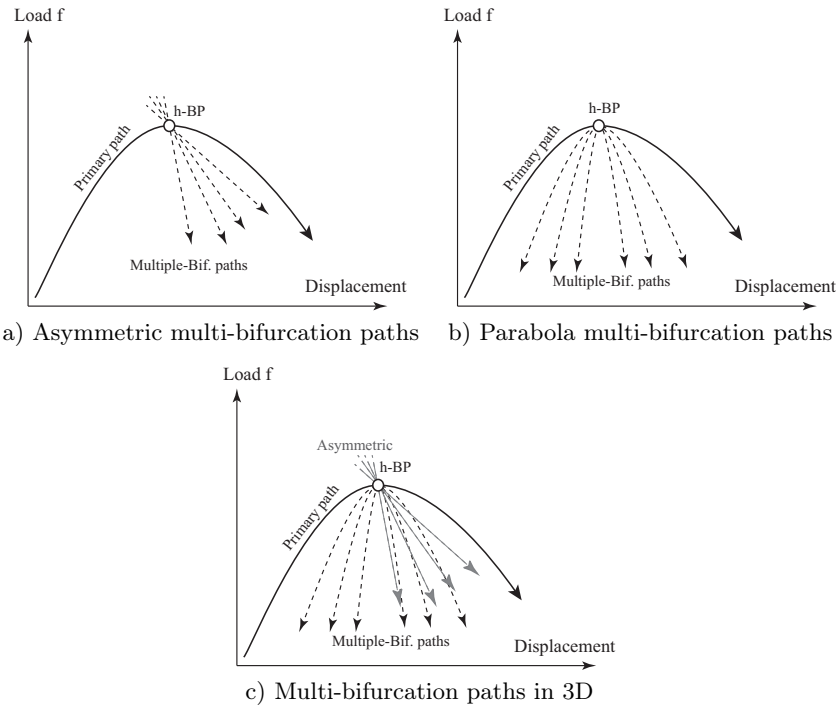

a) Asymmetric multi-bifurcation paths b) Parabola multi-bifurcation paths

c) Multi-bifurcation paths in 3D

FIG. 11. Classification of unstable multiple hilltop bifurcations.

it would seem more complicate than a bifurcation system where the real microstructure of the MFM system has many layers and degrees-of-freedom. In that case, there are evidences of the occurrence of more complex phenomena. However, this evidence is based on the diagram system for symmetry groups, considering the initial periodic symmetries of the MFM model.

4. Conclusion

This study clearly demonstrates, by using theoretical analysis, that there exist different bifurcation paths and primary nonlinear equilibrium paths in periodic structures. MFM truss models with multiple singularities were used. In this approach, the following conclusions are obtained based on the analytical results;

1. The existence of stable and unstable types, as well as the existence of symmetric and asymmetric systems at the h-BP, is recognized. This nonlinear phenomenon is essential for the stability of the periodic structure system, considering its microstructure. Moreover, it is also important when considering the stability of the folding mechanism that limits the holding support of a real structure, such as a deployable periodic structure.

2. Regarding a folding truss model (2D plane) of an m-layer pantograph, there exist multiple bifurcation points. Considering the stability analysis of the *Jacobian*, where multiple null eigenvalues occur at a certain critical displacement. It was found that there were multiple bifurcation points of the hilltop type and different bifurcation paths, when the number of layers m in the periodic MFM system was either odd or even.
3. The bifurcation behaviour of an elastic multi-layer MFM truss model such as a core truss with a diamond-shaped axisymmetric space truss in 3D, was elucidated in terms of its folding mechanism. The bifurcation paths with the regular n gonal space truss were derived from h-BP by n bifurcation paths. This indicates that the m-layers in the MFM, which has a large degree of freedom, has abundant branching paths. Furthermore, it was found that the derivation of branching path from the main one is technically quite difficult, and the more the number of 0 eigenvalues is, the more severe the stiffness decrease. The equilibrium equations were compared and investigated, by analysing different bifurcation paths, based on the symmetric group.
4. The geometrical symmetry of the truss was an important singularity of this simplified model, resulting in the occurrence of unstable deformation that disrupted the periodic symmetry. Therefore, the results of this study clarify the classification and invariance of multiple singularities in periodic structures.
5. In this paper, it was not available to obtain bifurcation hierarchy or more complex folding patterns of the multiple layers in the MFM. Therefore, further analysis including the more multi-degrees of freedom and/or the imperfection sensitivity variation will be necessary.

Acknowledgements

We would like to thank the reviewers for their highly scientific and informative comments on the manuscript for this paper. This research is indirectly supported by the Grant-in-Aid for Challenging Exploratory Research of the Japan Society for the Promotion of Science; KAKENHI Grant Number JP18K18888.

A part of this manuscript was presented at the conference of CMM 2019.

References

1. L.J. Gibson, M.F. Ashby, *Cellular Solids – Structure and Properties*, 2nd ed., Cambridge University Press, Cambridge, 1997.
2. C. Combescure, P. Henry, R.S. Elliott, *Post-bifurcation and stability of a finitely strained hexagonal honeycomb subjected to equi-biaxial in-plane loading*, International Journal of Solids and Structures, **88-89**, 296–318, 2016.

3. S. PAPKA, S. KYRIAKIDES, *Biaxial crushing of honeycombs – part I: experiments*, International Journal of Solids Structures, **36**, 29, 4367–4396, 1999a.

4. S. PAPKA, S. KYRIAKIDES, *Biaxial crushing of honeycombs – part II: analysis*, International Journal of Solids and Structures, **36**, 29, 4397–4423, 1999b.

5. N. OHNO, D. OKUMURA, H. NOGUCHI, *Microscopic symmetric bifurcation condition of cellular solids based on a homogenization theory of finite deformation*, Journal Mechanics and Physics of Solids, **50**, 1125–1153, 2002.

6. D. OKUMURA, N. OHNO, H. NOGUCHI, *Elastoplastic microscopic bifurcation and post-bifurcation behavior of periodic cellular solids*, Journal Mechanics and Physics of Solids, **52**, 641–666, 2004.

7. I. SAIKI, K. TERADA, K. IKEDA, M. HORI, *Appropriate number of unit cells in a representative volume element for micro-structural bifurcation encountered in a multi-scale modeling*, Computer Methods in Applied Mechanics and Engineering, **191**, 23-24, 2561–2585, 2002.

8. I. ARIO, T. YAMASHITA, Y. CHIKAHIRO, M. NAKAZAWA, F. KRZYSZTOF, C. GRACZYKOWSKI, P. PAWŁOWSKI, *Structural analysis of a scissor atructure*, Bulletin of the Polish Academy of Sciences: Technical Sciences, accepted and preprinting in 2020.

9. I. ARIO, A. WATSON, *Dynamic folding analysis for multi-folding structures under impact loading*, International Journal of Sound and Vibration, **308**, 3-5, 591–598, 2007.

10. J. HOLNICKI-SZULC, P. PAWŁOWSKI, M. WIKLO, *High-performance impact absorbing materials – the concept, design tools and applications*, Smart Materials and Structures, **12**, 461–467, 2003.

11. I. ARIO, M. NAKAZAWA, *Non-linear dynamic behaviour of multi-folding microstructure systems based on origami skill*, International Journal of Non-Linear Mechanics, **45**, 337–347, 2010.

12. I. ARIO, *Multiple Duffing problem in a folding structure with hilltop bifurcation and possible imperfections*, Meccanica, **49**, 8, 1967–1983, 2014.

13. K. MUROTA, K. IKEDA, *Computational use of group theory in bifurcation analysis of symmetric structures*, SIAM, Journal on Scientific and Statistical Computing, **12**, 2, 273–297, 1991.

14. K. MUROTA, K. IKEDA, *On randam imperfections for structures of regular-polygonal symmetry*, SIAM, Journal on Applied Mathematics, **52**, 6, 1780–1803, 1992.

15. K. IKEDA, K. MUROTA, H. FUJII, *Bifurcation hierarchy of symmetric structures*, International Journal of Solids and Structures, **27**, 12, 1551–1573, 1991.

16. K. IKEDA, K. MUROTA, *Bifurcation analysis of symmetric structures using block-diagonalization*, Computer Methods in Applied Mechanics and Engineering, **86**, 2, 215–243, 1991.

17. K. IKEDA, I. ARIO, K. TORII, *Block-diagonalization analysis of symmetric plates*, International Journal of Solids and Structures, **29**, 22, 2779–2793, 1992.

18. K. IKEDA, K. OIDE, K. TERADA, *Imperfection sensitive variation of critical loads at hilltop bifurcation point*, International Journal of Engineering Science, **40**, 743–772, 2002.

19. K. Ikeda, M. Ohsaki, Y. Kanno, *Imperfection sensitivity of hilltop branching points of systems with dihedral group symmetry*, International Journal of Non-Linear Mechanics, **40**, 755–774, 2005.

20. M. Ohsaki, K. Ikeda, *Imperfection sensitivity of degenerate hilltop branching points*, International Journal of Non-Linear Mechanics, **44**, 3, 324–336, 2009.

21. I. Ario, *Homoclinic bifurcation and chaos attractor in elastic two-bar truss*, International Journal of Non-Linear Mechanics, **39**, 4, 605–617, 2004.

22. I. Ario, A. Watson, *Dynamic folding analysis for multi-folding structures under impact loading*, Journal of Sound and Vibration, **308**, 3-5, 591–598, 2007.

23. I. Ario, A. Watson, *Structural stability of multi-folding structures with contact problem*, Journal of Sound and Vibration, **324**, 263–282, 2009.

24. J.M.T. Thompson, G.W. Hunt, *A General Theory of Elastic Stability*, Wiley, London, 1973.

25. Z.P. Bažant, L. Cedolin, *Stability of Structures, Elastic, Inelastic, Fracture, and Damage Theories*, Oxford Engineering Science Series, Oxford, 1990.

Received November 20, 2019; revised version May 25, 2020.
Published online August 10, 2020.